

# Linköping University Post Print

## Influence of phantom material and dimensions on experimental Ir-192 dosimetry

Åsa Carlsson Tedgren and Gudrun Alm Carlsson

N.B.: When citing this work, cite the original article.

Original Publication:

Åsa Carlsson Tedgren and Gudrun Alm Carlsson, Influence of phantom material and dimensions on experimental Ir-192 dosimetry, 2009, MEDICAL PHYSICS, (36), 6, 2228-2235.

<http://dx.doi.org/10.1118/1.3121508>

Copyright: American Institute of Physics

<http://www.aip.org/>

Postprint available at: Linköping University Electronic Press

<http://urn.kb.se/resolve?urn=urn:nbn:se:liu:diva-19421>

# Influence of phantom material and dimensions on experimental $^{192}\text{Ir}$ dosimetry

Åsa Carlsson Tedgren<sup>a)</sup> and Gudrun Alm Carlsson

Department of Medical and Health Sciences (IMH), Radiation Physics, Faculty of Health Sciences, Linköping University, SE-581 85 Linköping, Sweden

(Received 29 July 2008; revised 31 March 2009; accepted for publication 31 March 2009; published 18 May 2009)

In treatment planning of brachytherapy, absorbed dose is calculated by superposing predetermined distributions of absorbed dose to water in water for the single source according to the irradiation pattern [i.e., placement of the source(s) or dwelling position(s)]. Single-source reference water data are derived from Monte Carlo (MC) simulations and/or experiments. For reasons of positional accuracy, experimental brachytherapy dosimetry is most often performed in plastic phantoms. This work investigates the water equivalence of phantoms made from polystyrene, PMMA, and solid water for  $^{192}\text{Ir}$  dosimetry. The EGSnrc MC code is used to simulate radial absorbed dose distributions in cylindrical phantoms of dimensions ranging in size from diameter and height of 20 cm to diameter and height of 40 cm. Water equivalence prevails if the absorbed dose to water in the plastic phantom is the same as the absorbed dose to water in a water phantom at equal distances from the source. It is shown that water equivalence at a specified distance from the source depends not only on the size of the plastic phantom but also on the size of the water phantom used for comparison. Compared to equally sized water phantoms, phantoms of polystyrene are less water equivalent than phantoms of PMMA and solid water but compared to larger water phantoms they are the most water equivalent. Although phantom dimension is the most important single factor influencing the dose distributions around  $^{192}\text{Ir}$  sources, the effect of material properties is non-negligible and becomes increasingly important as phantom dimensions increase. The importance of knowing the size of the water phantom whose data underlies treatment planning systems, when using such data as a reference in, e.g., detector evaluation studies, is discussed. To achieve the highest possible accuracy in experimental dosimetry, phantom-specific correction factors should be used. © 2009 American Association of Physicists in Medicine. [DOI: [10.1118/1.3121508](https://doi.org/10.1118/1.3121508)]

Key words:  $^{192}\text{Ir}$ , dosimetry, plastic phantom, water equivalence

## I. INTRODUCTION

Brachytherapy dose calculation for treatment planning superposes single-source dose distributions in liquid water (in the following called water). For low energy seeds (i.e., sources with mean energies below 50 keV), Task Group No. 43 of the American Association of Physicists in Medicine (AAPM TG43-U1) recommends that results from one Monte Carlo (MC) and one experimental study be published before taking a source into clinical use and provides detailed specifications on how to derive such data.<sup>1</sup> For new  $^{192}\text{Ir}$  sources of design similar to existing ones, it is considered sufficient to conduct either a MC or an experimental study and compare the results with those from older source models.<sup>2</sup> Renewed interest in experimental  $^{192}\text{Ir}$  dosimetry is demonstrated in the design of dosimeters suitable for verifying treatment plans<sup>3</sup> or for *in vivo* dosimetry.<sup>4</sup>

Experimental brachytherapy dosimetry is a challenge due to steep gradients in dose and dose rate, low photon energies, and spectral changes with distance from the source. Since positional accuracy is crucial, measurements are often performed in plastic phantoms. To measure absorbed dose to water valid for points in a reference water phantom using plastic phantoms, these must be either truly water-equivalent or investigators must apply appropriate correction factors.

Several investigations have been performed on phantom materials for  $^{125}\text{I}$  and  $^{103}\text{Pd}$  seeds. The importance of the photoelectric effect at these low energies makes dose distributions highly sensitive to phantom composition<sup>5-7</sup> and material specific correction factors are required. The higher mean energy of the  $^{192}\text{Ir}$  photon spectrum makes dose distributions around  $^{192}\text{Ir}$  sources less sensitive to phantom composition and Meli *et al.*<sup>8</sup> concluded that for experimental  $^{192}\text{Ir}$  dosimetry, polystyrene and solid water can be considered water equivalent. Meli *et al.*<sup>8</sup> also found that under conditions of “full scatter,” defined as the presence of at least 5 cm of material exterior to the point of measurement, PMMA was water equivalent. The results by Meli *et al.*<sup>8</sup> are still referenced to indicate the water equivalence of phantom materials for  $^{192}\text{Ir}$  dosimetry.<sup>9</sup>

Meli *et al.*<sup>8</sup> based their conclusion as to the water equivalence of PMMA, polystyrene, and solid water on the results of experiments and MC simulations without studying the impact of varying phantom dimensions. The influence of phantom size on radial dose distributions around  $^{192}\text{Ir}$  sources in water was investigated by Ellett<sup>10</sup> and later by Pérez-Calatayud *et al.*,<sup>11</sup> with extensions to various tissue materials by Melhus and Rivard.<sup>12</sup> The influence of phantom dimensions on experimental  $^{192}\text{Ir}$  dosimetry was pointed out by

Williamson<sup>13</sup> who found improved agreement between MC and experimental results when the MC simulations were performed for the measurement geometry used. Recently, Granero *et al.*<sup>14</sup> investigated how radial absorbed dose distributions depend on the sizes and shapes of the water phantoms used. They further provide readers with information necessary to compare radial dose profiles of data sets derived in water phantoms of different sizes and shapes.

The aim of this work is to investigate further the water equivalence of various plastic phantoms regarding their use in experimental  $^{192}\text{Ir}$  dosimetry. A situation of special interest is that of experiments performed to verify MC results for single-source reference water data underlying treatment planning dose calculations. The sizes of water phantoms used in MC studies vary between investigations as do the sizes of the plastic phantoms used in the experiments. The single-source geometry investigated by Meli *et al.*<sup>8</sup> is in this work extended to study the water equivalence of plastic phantoms compared to both similarly and differently sized water phantoms.

## II. THEORY

### II.A. Water equivalence

In cases when charged particle equilibrium can be assumed, absorbed dose to water calculated at points in a water phantom is given by the water collision kerma. This is a valid approximation for photon energies below 1 MeV and can be assumed for photon energies used in brachytherapy. Using a plastic phantom, we assumed that the absorbed dose to water at a point in the phantom is given by the water collision kerma at that point. This is the same as assuming that a small dosimeter of water in which charged particle equilibrium prevails is positioned at that point. A plastic phantom is then said to be water equivalent if the absorbed dose to water at a point in the phantom is equal to the absorbed dose to water in a water phantom at (on a linear scale) equal distances from the source over the specified range of measurements.

The absorbed dose to water in a water phantom is denoted  $D_{w,w}$ , the absorbed dose to water in a plastic phantom  $D_{w,\text{phan}}$ , and the absorbed dose to the phantom material in the phantom  $D_{\text{phan,phan}}$ . Using this formalism, water equivalence of a phantom means that  $D_{w,\text{phan}} = D_{w,w}$  at all points in the phantom.

In MC simulations, the absorbed dose to the phantom material,  $D_{\text{phan,phan}}$ , is primarily calculated. Assuming charged particle equilibrium, this can be expressed as

$$D_{\text{phan,phan}} = \int_0^{h\nu_{\text{max}}} \left( \frac{\mu_{\text{en}}(h\nu)}{\rho} \right)_{\text{phan}} \Psi_{\text{phan}}(h\nu) dh\nu. \quad (1)$$

Here,  $\Psi_{\text{phan}}(h\nu)dh\nu$  is the energy fluence of photons with energies in the interval  $h\nu, h\nu+dh\nu$  and  $(\mu_{\text{en}}/\rho)_{\text{phan}}$  is the mass-energy absorption coefficient for the phantom material. The absorbed dose to water in the water phantom is given by Eq. (1) with the index phan for the phantom replaced by index  $w$  for water.

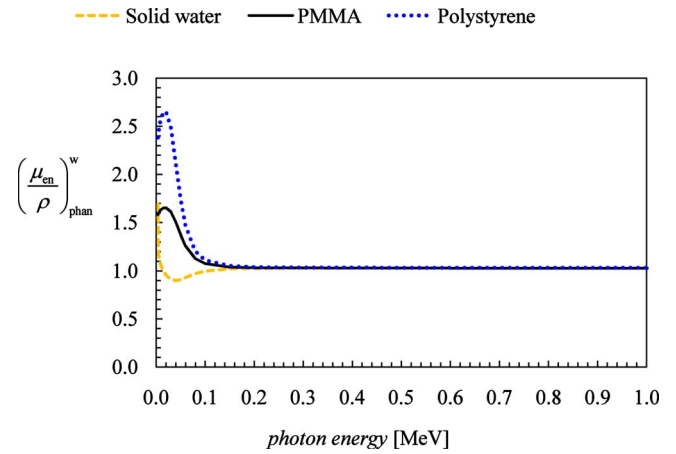


FIG. 1. Ratios of mass-energy absorption coefficients,  $(\mu_{\text{en}}/\rho)_{\text{phan}}^w$ , between water and the investigated phantom materials as a function of photon energy. The atomic compositions of the materials are given in Table I.

The absorbed dose to water at a point in the phantom is then obtained from

$$\begin{aligned} D_{w,\text{phan}} &= \frac{\int_0^{h\nu_{\text{max}}} \left( \frac{\mu_{\text{en}}(h\nu)}{\rho} \right)_w \Psi_{\text{phan}}(h\nu) dh\nu}{\int_0^{h\nu_{\text{max}}} \left( \frac{\mu_{\text{en}}(h\nu)}{\rho} \right)_{\text{phan}} \Psi_{\text{phan}}(h\nu) dh\nu} \cdot D_{\text{phan,phan}} \\ &= \frac{\left( \frac{\bar{\mu}_{\text{en}}}{\rho} \right)_w \Psi_{\text{phan}}}{\left( \frac{\bar{\mu}_{\text{en}}}{\rho} \right)_{\text{phan}} \Psi_{\text{phan}}} \cdot D_{\text{phan,phan}} \\ &= \left( \frac{\bar{\mu}_{\text{en}}}{\rho} \right)_{\text{phan}}^w \cdot D_{\text{phan,phan}}. \end{aligned} \quad (2)$$

Equation (2) shows that  $(\bar{\mu}_{\text{en}}/\rho)_{\text{phan}}^w$  is the quotient of energy fluence weighted means of the mass-energy absorption coefficients for water and phantom material, respectively. The distribution of the photon energy fluence to calculate  $(\bar{\mu}_{\text{en}}/\rho)_{\text{phan}}^w$  can be derived from MC simulations, as shown in Sec. III.A.

In Fig. 1, the quotients of the mass-energy absorption coefficients,  $(\mu_{\text{en}}/\rho)_{\text{phan}}^w$ , for the phantom materials investigated are shown as functions of photon energy. The energy dependence in ratios of mass-energy absorption coefficients between water and the investigated plastics increases substantially below 100 keV and is most pronounced for polystyrene.

### II.B. Examples of phantoms used in experimental and MC $^{192}\text{Ir}$ dosimetry

There exist numerous publications on single-source  $^{192}\text{Ir}$  reference data from various manufacturers; for an overview see Ref. 15. Of these, a few present both MC simulations and experimental measurements (or relate the two to each other). Kirov *et al.*<sup>16</sup> compared MC simulations of a  $^{192}\text{Ir}$  high dose rate (HDR) source in a spherical water phantom of radius 15 cm to experimental thermoluminescent (TL) dosimetry per-

formed in a rectangular ( $28 \times 28 \times 20 \text{ cm}^3$ ) phantom of solid water. MC simulations in a spherical water phantom of radius 15 cm by Williamson and Li<sup>17</sup> were experimentally verified by Valicenti *et al.*<sup>18</sup> in a rectangular solid water phantom (dimensions  $28 \times 28 \times 20 \text{ cm}^3$ ). Karaikos *et al.*<sup>19</sup> compared MC simulations in a spherical water phantom of radius 15 cm to experimental TL dosimetry in a cubic polystyrene phantom (dimensions  $30 \times 30 \times 30 \text{ cm}^3$ ).

In MC studies, some investigators have followed the TG-43U1 recommendation<sup>1</sup> of using a spherical water phantom of radius 15 cm,<sup>16–19</sup> while others have used cylindrical water phantoms of radius 20 cm and height 40 cm (Refs. 20–22) or larger.<sup>23</sup> Current trends support the use of large phantoms, providing full scatter within a radius of 20 cm from the source.<sup>11</sup> A recent comprehensive MC study<sup>15</sup> presenting single-source data on all available  $^{192}\text{Ir}$  HDR and PDR sources used a cubic water phantom of dimensions  $80 \times 80 \times 80 \text{ cm}^3$ . The MC component of the work by Meli *et al.*<sup>8</sup> used a cylindrical phantom of radius 15 cm and height 10 cm.

Some experimental studies do not provide the exact dimensions of the plastic phantoms used but only specify “full scattering conditions,” for examples see the overview by Ghiassi-Nejad *et al.*<sup>24</sup> The water phantom used in the experimental component of the work by Meli *et al.*<sup>8</sup> was a Scanditronix Therados RFA-3 tank. The water height within the  $60 \times 60 \times 60 \text{ cm}^3$  phantom was not provided. The sizes of the plastic phantoms by Meli *et al.*<sup>8</sup> were  $20 \times 20 \times 20 \text{ cm}^3$ . However, additional slabs were sometimes used to increase the phantom height to allow larger source-detector (ion chamber) distances to maintain at least 7 cm of phantom material surrounding both source and detector.

### III. MATERIALS AND METHODS

#### III.A. MC simulations

MC simulations were performed using EGSnrc version V4-r2-2-5.<sup>25</sup> A point source was modeled and given a photon energy spectrum supplied with the EGSnrc package, corresponding to that in air at  $90^\circ$  with the longitudinal axis just outside a steel-encapsulated microSelectron-v1 HDR  $^{192}\text{Ir}$  source.<sup>26</sup> The design and materials in other HDR and PDR  $^{192}\text{Ir}$  sources are similar and results obtained using this spectrum should be representative of similar sources from other manufacturers.<sup>15</sup> Simulations were performed using both DOSRZnrc and FLURZnrc, user codes supplied with EGSnrc (Ref. 27) for scoring absorbed dose and fluence differential in energy (i.e., energy spectra) in cylindrical geometries. Three differently sized cylindrical phantoms (heights of 20, 30, and 40 cm and radii of 10, 15, and 20 cm, respectively) were modeled and filled with either water, PMMA, polystyrene, or solid water. The atomic compositions of the materials are listed in Table I. For improved modeling of low energy photons, XCOM cross sections<sup>28</sup> compiled for use with EGSnrc were used.<sup>29</sup> Rayleigh scattering, Compton interactions with bound electrons, and atomic relaxation after photoelectric events were modeled. The cut-off energy for photon transport was 1 keV. Electron transport was not mod-

TABLE I. Atomic compositions of the materials used in the EGSnrc MC simulations.

Element	Water (No. of atoms per molecule)	PMMA (No. of atoms per molecule)	Solid water (fraction by weight, %)	Polystyrene (fraction by weight, %)
H	2	5	8.09	7.74
C	–	8	67.22	92.26
O	1	2	19.84	–
N	–	–	2.40	–
Al	–	–	2.32	–
Cl	–	–	0.13	–
Density ( $\text{g cm}^{-3}$ )	1.00	1.19	1.03	1.06

eled. The number of simulated photon histories was  $5 \times 10^8$ , which ensured a standard deviation in absorbed dose of less than 0.5% for all the distances and phantom sizes studied.

For all materials and phantom sizes studied, simulations were performed with the point source placed centrally in the phantoms (i.e., at  $z=0$  and  $r=0$ ). Absorbed dose was scored along the central radius of the phantom in cylindrical voxels of dimensions ( $\Delta r=0.2 \text{ cm}$ ,  $\Delta z=0.1 \text{ cm}$ ). Fluence spectra were scored in 10 keV energy bins using cylindrical voxels of dimensions ( $\Delta r=0.2 \text{ cm}$ ,  $\Delta z=0.1 \text{ cm}$ ) that were centered at 1, 3, 5, 7, 9, 11, 13, 15, 17, and 19 cm along the central radius. The  $(\bar{\mu}_{\text{en}}/\rho)_{\text{phan}}^w$  in Eq. (2) was derived by numerically averaging mass-energy absorption coefficients over the energy fluence spectra. Tables of mass-energy absorption coefficients from Hubbell and Seltzer<sup>30</sup> were used. Logarithmic interpolation in the tables was applied to obtain values at the energies of the spectra used.

#### III.B. Data handling

The MC derived values of  $D_{\text{phan,phan}}$  were multiplied by the square of the radial distance from the source. The resulting radial dose profiles were fitted to fifth-order polynomials. MC derived energy fluence spectra were used to derive  $(\bar{\mu}_{\text{en}}/\rho)_{\text{phan}}^w$  [Eq. (2)] as a function of radial distance from the source and fitted to fifth-order polynomials. Use of polynomial fits to represent  $D_{\text{phan,phan}}$  eliminated the influence of statistical noise on absorbed dose values. Another advantage of using polynomial fits to represent  $D_{\text{phan,phan}}$  and  $(\bar{\mu}_{\text{en}}/\rho)_{\text{phan}}^w$  as functions of depth is that this made it possible to continuously convert values of  $D_{\text{phan,phan}}$ , obtained in MC simulations, to  $D_{w,\text{phan}}$ , required to test water equivalence (defined as  $D_{w,\text{phan}}=D_{w,w}$ ). The polynomials were never used outside the input data range.

## IV. RESULTS

#### IV.A. Fluence energy spectra

Figures 2(a) and 2(b) show photon fluence energy spectra at 7 cm from the source for equally sized water, PMMA, polystyrene, and solid water phantoms. Results are shown

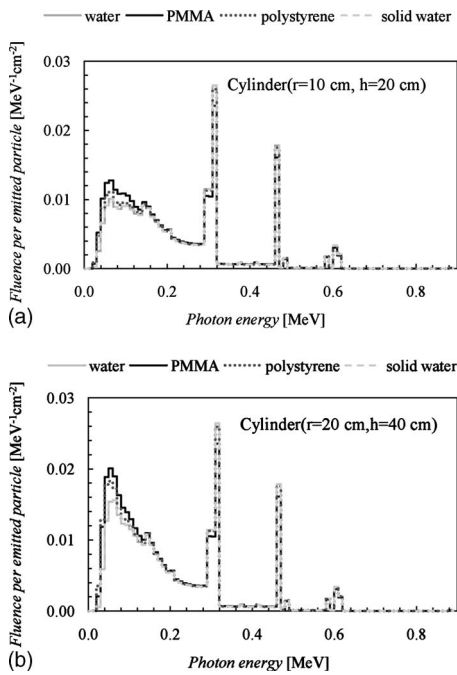


FIG. 2. (a) Photon fluence energy spectra at 7 cm on the central axis from the source in cylindrical water, PMMA, polystyrene, and solid water phantoms of radii 10 cm and heights 20 cm, normalized per particle emitted from a point source positioned at the centers of the phantoms. (b) Photon fluence energy spectra at 7 cm on the central radius from the source in cylindrical water, PMMA, polystyrene, and solid water phantoms of radii 20 cm and heights 40 cm, normalized per particle emitted from a point source positioned at the centers of the phantoms.

for two differently sized phantoms: Cylinders of radius 10 cm and height 20 cm [Fig. 2(a)] and of radius 20 cm and height 40 cm [Fig. 2(b)].

The influence of phantom dimensions on the energy spectra at 7 cm is seen by the substantially higher fluence of low energy scattered photons in the larger phantom. The fluence of primary photons is similar in water and polystyrene while that in PMMA is significantly lower. The higher density of PMMA results in a higher attenuation of primary photons that is associated with a corresponding increase in the buildup of scattered photons. In the smaller phantom [Fig. 2(a)], the fluence of scattered photons is similar in water and polystyrene; in the larger phantom, however, the fluence of low energy photons in polystyrene approaches that in PMMA. While polystyrene is closer to water in density than PMMA, the lower atomic numbers of its constituents result in a larger fraction of scattered photons. This increase in low energy photon fluence is more pronounced for the larger phantom. Spectra in water and solid water are indistinguishable in both phantoms.

#### IV.B. Ratios of mass-energy absorption coefficients for differently sized phantoms

Values of  $(\bar{\mu}_{\text{en}}/\rho)_{\text{phan}}^w$  for the centrally positioned source and various phantom materials are shown as functions of distance along the central radius of the phantoms in Fig. 3, together with the corresponding polynomial fits. The differ-

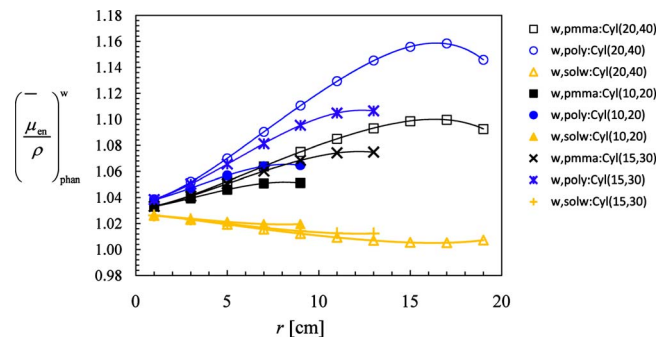


FIG. 3. Ratios of mass-energy absorption coefficients of water and phantom materials,  $(\bar{\mu}_{\text{en}}/\rho)_{\text{phan}}^w$ , averaged over the energy spectra [Eq. (2)] along the central radius of the phantom, as a function of distance  $r$  from the centrally positioned point source. Dimensions (in cm) of the cylindrical phantom (radius, height) are the parameters specified in the legend.

ence in the values for the same material with phantom size is a result of differences in photon energy spectra at equal distances from the source in phantoms of different dimensions [for  $r=7$  cm, see Figs. 2(a) and 2(b)]. The larger the phantom, the lower is the mean energy of the photons caused by increased fractions of scattered, energy-degraded photons. The energy absorption properties of polystyrene in relation to water (see Fig. 1) make measurements of absorbed dose in polystyrene more sensitive to variations in energy spectra than measurements performed in PMMA or solid water.

#### IV.C. Water equivalence of plastic phantoms

##### IV.C.1. Water equivalence of plastic phantoms in relation to water phantoms of equal size

To isolate the influences of material properties from those of phantom dimensions, the water equivalence (expressed by the dose ratio  $D_{w,\text{phan}}/D_{w,w}$ ) of the plastic phantoms at points along their central radius has been evaluated in comparison to water phantoms of the same size. Results are shown in Figs. 4(a)–4(c).

For the smallest phantom, polystyrene is water equivalent to within 1% [Fig. 4(a)]. When dimensions are increased, however, the degree of water equivalence is reduced to within +2% at 5 cm, +4% at 10 cm for the intermediately sized phantom [Fig. 4(b)], and to within +5.5% at 10 cm for the largest phantom [Fig. 4(c)].

PMMA is water equivalent to within  $\pm 1\%$  out to 7 cm in the smallest phantom [Fig. 4(a)] and out to 11.5 and 14 cm in the two larger ones, respectively [Figs. 4(b) and 4(c)]. The water equivalence of PMMA is increasingly lost at the edges of the phantoms since the faster attenuation in PMMA (caused by its approximately 20% higher density than water) is not compensated for by the buildup of scattered photons, in agreement with findings reported by Meli *et al.*<sup>8</sup>

Solid water is water equivalent to within  $-1\%$  in the smallest phantom [Fig. 4(a)]. In the two larger phantoms, water equivalence is to within  $-1\%$  out to 5 cm but decreases toward  $-2\%$  at 10 cm in both phantoms [Figs. 4(b) and 4(c)].

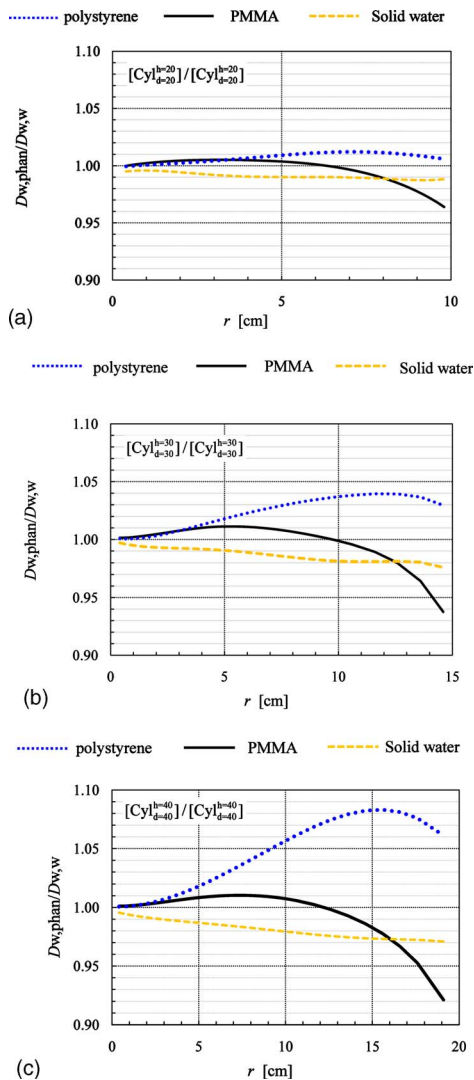


FIG. 4. (a) Ratios of absorbed dose to water in phantom ( $D_{w,\text{phan}}$ ) to absorbed dose to water in water phantom ( $D_{w,w}$ ) in equally sized cylindrical phantoms of diameter ( $d$ ) and height ( $h$ ) 20 cm along the central radius for a centrally positioned source. (b) Ratios of absorbed dose to water in phantom ( $D_{w,\text{phan}}$ ) to absorbed dose to water in water phantom ( $D_{w,w}$ ) in equally sized cylindrical phantoms of diameter ( $d$ ) and height ( $h$ ) 30 cm along the central radius for a centrally positioned source. (c) Ratios of absorbed dose to water in phantom ( $D_{w,\text{phan}}$ ) to absorbed dose to water in water phantom ( $D_{w,w}$ ) in equally sized cylindrical phantoms of diameter ( $d$ ) and height ( $h$ ) 40 cm along the central radius for a centrally positioned source.

#### IV.C.2. Water equivalence of plastic phantoms in relation to water phantoms of different sizes

*IV.C.2.a. Plastic phantom smaller than water phantom.* Figures 5(a) and 5(b) show the water equivalence of cylindrical plastic phantoms and a water phantom of diameter and height 20 cm in relation to cylindrical water phantoms of diameter and height 30 cm [Fig. 5(a)] and of diameter and height 40 cm [Fig. 5(b)]. Figure 5(c) shows the water equivalence of cylindrical plastic phantoms and a water phantom of diameter and height 30 cm in relation to a water phantom of diameter and height 40 cm.

The influence of phantom size alone can be seen by inspecting the dose ratios for the water phantoms. The water

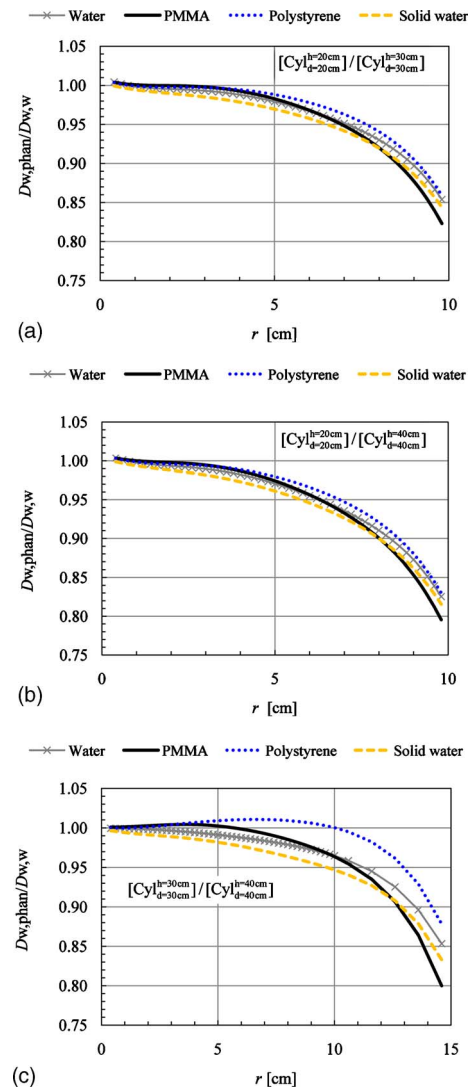


FIG. 5. (a) Ratios of absorbed dose to water in phantom ( $D_{w,\text{phan}}$ ) of diameter ( $d$ ) and height ( $h$ ) 20 cm to absorbed dose to water in a cylindrical water phantom of diameter and height 30 cm along the central radius in the phantoms for a centrally positioned source. (b) Ratios of absorbed dose to water in phantom ( $D_{w,\text{phan}}$ ) of diameter ( $d$ ) and height ( $h$ ) 20 cm to absorbed dose to water in a cylindrical water phantom of diameter and height 40 cm along the central radius in the phantoms for a centrally positioned source. (c) Ratios of absorbed dose to water in phantom ( $D_{w,\text{phan}}$ ) of diameter ( $d$ ) and height ( $h$ ) 30 cm to absorbed dose to water in a cylindrical water phantom of diameter and height 40 cm along the central radius in the phantoms for a centrally positioned source.

equivalence of the smallest water phantom in relation to the intermediate-sized one [Fig. 5(a)] is  $-0.5\%$  at 2.5 cm,  $-2\%$  at 5 cm, and  $-6\%$  at 7.5 cm from the source. Corresponding values for the intermediate-sized phantom in relation to the largest water phantom [Fig. 5(c)] are  $-1.5\%$  at 5 cm and  $-3.5\%$  at 10 cm from the source.

Interestingly, while polystyrene is less water equivalent than the other plastic phantoms in comparison to water phantoms of equal size [Figs. 4(a)–4(c)], it is the most water-equivalent one in relation to water phantoms of larger size [Figs. 5(a)–5(c)] including the water phantom of the same size as the polystyrene one. This is due to the lower atomic

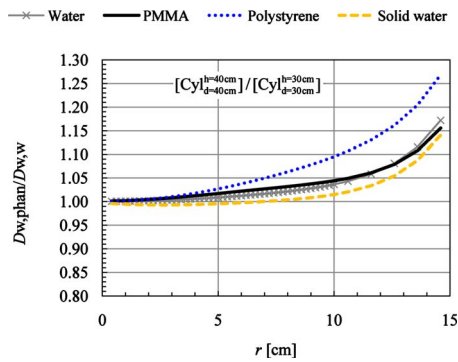


FIG. 6. Ratios of absorbed dose to water in phantoms ( $D_{w,\text{phan}}$ ) of diameter ( $d$ ) and height ( $h$ ) 40 cm to absorbed dose to water ( $D_{w,w}$ ) in a cylindrical water phantom of diameter and height 30 cm along the central radius of the phantoms and for a centrally positioned source.

numbers of polystyrene (hydrogen and carbon but no oxygen) which cause larger fractions of scattered photons in the polystyrene phantom, balancing the increased scatter in the larger water phantoms. The lack of water equivalence of the solid water phantoms seen in Fig. 4 for phantoms of equal size is further accentuated when the solid water phantom is smaller than the water phantom (Fig. 5).

*IV.C.2.b. Plastic phantom larger than water phantom.* Figure 6 shows the water equivalence of cylindrical plastic phantoms of diameter and height 40 cm (including a water phantom of equal size) in relation to a smaller cylindrical water phantom of diameter and height 30 cm. Figure 6 shows that solid water is more water equivalent than the other phantoms (including water) when compared to a smaller water phantom. Experimental plastic phantoms are generally smaller than reference water phantoms used in MC simulations. The results in Fig. 6 are, however, interesting since they complement those in Figs. 4 and 5, demonstrating how the differences in the scattering properties of various phantom materials (see Fig. 1) influence their water equivalence in a manner depending on phantom size in relation to the size of the reference phantom.

## V. DISCUSSION

It is not practical to construct experimental plastic phantoms of as large dimensions as those used in generating  $^{192}\text{Ir}$  single-source reference data with MC simulations ensuring full scatter out to 20 cm distance.<sup>11,15</sup> In addition, although size is the factor of largest influence, the choice of material cannot be disregarded. The difference between water and plastic is more pronounced for large phantoms, even when these are of the same sizes as the water reference phantoms [see Figs. 4(a)–4(c)].

Meli *et al.*<sup>8</sup> concluded that all the phantom materials investigated in their study were water equivalent for  $^{192}\text{Ir}$  dosimetry as long as at least 7 cm of material surrounded both source and detector. The good agreement between their measurements in the polystyrene and water phantoms may be

explained by the water phantom being larger than the polystyrene phantom used (see Sec. II.B), in agreement with our results in Fig. 5(c).

For equally sized phantoms, polystyrene is the least water-equivalent material, in particular, for the larger size of phantom in Fig. 4(c). At 7 cm from the phantom edge, the absorbed dose to water in the polystyrene phantom is about 8% higher than the absorbed dose to water in the water phantom, whereas the absorbed doses to water in the PMMA phantom are within 1% of those in the water phantom. The MC simulations by Meli *et al.* also showed good agreement between the absorbed doses obtained in polystyrene and water phantoms. This may be explained by the use of a comparatively small phantom (radius 15 cm, height 10 cm) in the simulations [see Fig. 4(a)]. Meli *et al.* did not compare their MC simulations and experiments except for water where depth doses normalized at 3 cm showed good agreement. The statistical precision in their simulated data was no better than 3% (1 standard deviation), corresponding to an expanded uncertainty of 6% at coverage factor  $k=2$ . In our work, discrepancies on the order of 6% or less are statistically significant since the standard deviation in absorbed dose data was less than 0.5% and, in addition, the data were smoothed by polynomial fitting. Our results show that in most of the cases studied, water equivalence within 6% is obtainable at distances up to 7 cm from the phantom edge except for the case with polystyrene and a large equally sized water phantom [Fig. 4(c)].

A situation of interest is when absorbed doses to water derived by treatment planning systems (TPSs) are to be verified experimentally or to be used as references in evaluating detector performance.<sup>31</sup> Experimental phantoms are usually cubic and commonly used TPSs use as references a water cylinder of diameter and height 40 cm (Varian for the GammaMed Plus and 12i sources<sup>20–22</sup>) or a water sphere of diameter 30 cm (Nucletron for all their sources<sup>17,32–34</sup>). Results<sup>14</sup> for water phantoms indicate that cubic phantoms with sides 20 and 30 cm correspond to cylinders of diameter and height 22 and 33 cm; a spherical phantom of diameter 30 cm corresponds to a cylinder of diameter and height 28 cm. Using this information it is, assuming dependence on shape to be similar for plastic and water phantoms, possible to roughly estimate corrections needed if data for cylindrical phantoms are used in measurements with cubic phantoms. To be representative of a cubic solid phantom with sides of 20 cm (30 cm) in relation to a cylindrical water phantom of height and diameter 40 cm, the quotients in Fig. 5(b) [Fig. 5(c)] have to be multiplied by the correction factors of Eqs. (3) and (4), respectively:

$$[\text{Cyl}_{d=22\text{ cm}}^{h=22\text{ cm}}/\text{Cyl}_{d=40\text{ cm}}^{h=40\text{ cm}}]_{w'}/[\text{Cyl}_{d=20\text{ cm}}^{h=20\text{ cm}}/\text{Cyl}_{d=40\text{ cm}}^{h=40\text{ cm}}]_{w}, \quad (3)$$

$$[\text{Cyl}_{d=33\text{ cm}}^{h=33\text{ cm}}/\text{Cyl}_{d=40\text{ cm}}^{h=40\text{ cm}}]_{w'}/[\text{Cyl}_{d=30\text{ cm}}^{h=30\text{ cm}}/\text{Cyl}_{d=40\text{ cm}}^{h=40\text{ cm}}]_{w}. \quad (4)$$

The factor of Eq. (3) is equal to +1% out to 6 cm, +2% at 8 cm, and +4% at 10 cm, while that of Eq. (4) is equal to +1%

out to 10 cm from the source. Corresponding correction factors to the quotients in Fig. 5(a) [Fig. 4(b)] which are representative of solid cubic phantoms with sides of 20 cm (30 cm) in relation to a spherical phantom with diameter of 30 cm are given in Eqs. (5) and (6):

$$[\text{Cyl}_{d=22}^{h=22} \text{ cm} / \text{Cyl}_{d=28}^{h=28} \text{ cm}]_{\text{w}} / [\text{Cyl}_{d=20}^{h=20} \text{ cm} / \text{Cyl}_{d=30}^{h=30} \text{ cm}]_{\text{w}}, \quad (5)$$

$$[\text{Cyl}_{d=33}^{h=33} \text{ cm} / \text{Cyl}_{d=28}^{h=28} \text{ cm}]_{\text{w}} / [\text{Cyl}_{d=30}^{h=30} \text{ cm} / \text{Cyl}_{d=30}^{h=30} \text{ cm}]_{\text{w}}. \quad (6)$$

The factor of Eq. (5) is +1% out to 4 cm and within +2% out to 6 cm, thereafter rapidly increasing toward +10% at 10 cm from the source. That of Eq. (6) is +0.5% out to 4 cm and within +2% out to 6 cm, thereafter rapidly increasing toward +6% at 10 cm from the source.

## VI. CONCLUSIONS

The degrees of water equivalence of plastic phantoms depend on phantom material and the sizes of the phantoms as well as the size of the water phantom used for comparison. While phantom size is the largest factor influencing water equivalence, the influence of phantom material is not negligible and increases with increasing phantom size. Use of phantom-specific correction factors is recommended for experiments which demand high accuracy such as those aiming to verify single-source treatment planning data or evaluating the performance of new detectors. In this context it is important to emphasize that the size of the water phantom used for deriving the single-source reference data is different in different treatment planning systems. Corrections to data derived in a cylindrical phantom of diameter and height 20 cm (30 cm) to represent a cubic phantom with sides 20 cm (30 cm) in relation to a cylindrical reference phantom of diameter and height 40 cm (used as reference water phantom in the Varian TPS) are about 1% out to 6–10 cm from the source (depending on phantom size). Corresponding corrections applied using data for cylindrical phantoms to represent cubic phantoms in relation to a spherical reference phantom (as that used in the Nucletron TPS) are larger. The need for phantom-specific correction factors will increase with the future use of even larger phantoms for MC simulations of reference water data.

Overall, PMMA is the most water-equivalent (for the sizes explored in this work) phantom material independent of the size of the water phantom used for comparison, except for the region 5–7 cm from the edge. Compared to water phantoms of larger size, polystyrene is the most water-equivalent material [Figs. 5(a)–5(c)]. Solid water is the most water-equivalent material when compared to water phantoms of smaller dimensions (Fig. 6).

The energy spectrum of the photon fluence in a given phantom position in multiple-source irradiation is not identical to that around a single source. We recommend that experimental investigators bear in mind that the water equivalence of a given phantom in single-source irradiation might therefore not be the same in multiple-source irradiations.

## ACKNOWLEDGMENT

This work was supported by grants from the Swedish Cancer Foundation (CF), Contract No. 07 0621.

<sup>a)</sup>Electronic mail: asa.carlsson-tedgren@imv.liu.se

<sup>1</sup>M. J. Rivard, B. M. Coursey, L. A. DeWerd, W. F. Hanson, M. S. Huq, G. S. Ibbott, M. G. Mitch, R. Nath, and J. F. Williamson, "Update of AAPM Task Group No. 43 Report: A revised AAPM protocol for brachytherapy dose calculations," *Med. Phys.* **31**, 633–674 (2004).

<sup>2</sup>Z. Li, R. K. Das, L. A. DeWerd, G. S. Ibbott, A. S. Meigooni, J. Pérez-Calatayud, M. J. Rivard, R. S. Sloboda, and J. F. Williamson, "Dosimetric prerequisites for routine clinical use of photon emitting brachytherapy sources with average energy higher than 50 keV," *Med. Phys.* **34**, 37–40 (2007).

<sup>3</sup>Z. Qi, X. Deng, S. Huang, J. Lu, M. Lerch, D. Cutajar, and A. Rosenfeld, "Verification of the plan dosimetry for high dose rate brachytherapy using metal-oxide-semiconductor field effect transistor detectors," *Med. Phys.* **34**, 2007–2013 (2007).

<sup>4</sup>J. Lambert, T. Nakano, S. Law, J. Elsey, D. R. McKenzie, and N. Suchowerska, "In vivo dosimeters for HDR brachytherapy: A comparison of a diamond detector, MOSFET, TLD, and scintillator detector," *Med. Phys.* **34**, 1759–1765 (2007).

<sup>5</sup>A. S. Meigooni, J. A. Meli, and R. Nath, "A comparison of solid phantoms with water for dosimetry of  $^{125}\text{I}$  brachytherapy sources," *Med. Phys.* **15**, 695–701 (1988).

<sup>6</sup>B. Reniers, F. Verhaegen, and S. Vynckier, "The radial dose function of low-energy brachytherapy seeds in different solid phantoms: Comparison between calculations with the EGSnrc and MCNP4C Monte Carlo codes and measurements," *Phys. Med. Biol.* **49**, 1569–1582 (2004).

<sup>7</sup>N. S. Patel, S. Chiu-Tsao, J. F. Williamson, P. Fan, T. Duckworth, D. Shasha, and L. B. Harrison, "Thermoluminescent dosimetry of the Symmetra™  $^{125}\text{I}$  model I25.06 interstitial brachytherapy seed," *Med. Phys.* **28**, 1761–1769 (2001).

<sup>8</sup>J. A. Meli, A. S. Meigooni, and R. Nath, "On the choice of phantom material for the dosimetry of  $^{192}\text{Ir}$  sources," *Int. J. Radiat. Oncol., Biol., Phys.* **14**, 587–594 (1988).

<sup>9</sup>J. F. Williamson and M. J. Rivard, in *Brachytherapy Physics*, edited by B. R. Thomadsen, M. J. Rivard, and W. M. Butler (Medical Physics, Madison, 2005), Chap. 15, pp. 233–294.

<sup>10</sup>W. H. Ellett, "Specific absorbed fractions for photon point sources within a scattering medium," *Phys. Med. Biol.* **14**, 615–626 (1969).

<sup>11</sup>J. Pérez-Calatayud, D. Granero, and F. Ballester, "Phantom size in brachytherapy source dosimetric studies," *Med. Phys.* **31**, 2075–2081 (2004).

<sup>12</sup>C. S. Melhus and M. J. Rivard, "Approaches to calculating AAPM TG-43 brachytherapy dosimetry parameters for  $^{137}\text{Cs}$ ,  $^{125}\text{I}$ ,  $^{192}\text{Ir}$ ,  $^{103}\text{Pd}$  and  $^{169}\text{Yb}$  sources," *Med. Phys.* **33**, 1729–1737 (2006).

<sup>13</sup>J. F. Williamson, "Comparison of measured and calculated dose rates in water near I-125 and Ir-192 seeds," *Med. Phys.* **18**, 776–786 (1991).

<sup>14</sup>D. Granero, J. Pérez-Calatayud, M. Pujades-Claumarchirant, F. Ballester, C. Melhus, and M. J. Rivard, "Equivalent phantom sizes and shapes for brachytherapy dosimetric studies of  $^{192}\text{Ir}$  and  $^{137}\text{Cs}$ ," *Med. Phys.* **35**, 4872–4877 (2008).

<sup>15</sup>R. E. P. Taylor and D. W. O. Rogers, "EGSnrc Monte Carlo calculated dosimetry parameters for  $^{192}\text{Ir}$  and  $^{169}\text{Yb}$  sources," *Med. Phys.* **35**, 4933–4944 (2008).

<sup>16</sup>A. S. Kirov, J. F. Williamson, A. S. Meigooni, and Y. Zhu, "TLD, diode and Monte Carlo dosimetry of an  $^{192}\text{Ir}$  source for high dose-rate brachytherapy," *Phys. Med. Biol.* **40**, 2015–2036 (1995).

<sup>17</sup>J. F. Williamson and Z. Li, "Monte Carlo aided dosimetry of the microelectron pulsed and high dose-rate  $^{192}\text{Ir}$  sources," *Med. Phys.* **22**, 809–819 (1995).

<sup>18</sup>R. K. Valicenti, A. S. Kirov, A. S. Meigooni, V. Mishra, R. K. Das, and J. F. Williamson, "Experimental validation of Monte Carlo dose calculations about a high-intensity Ir-192 source for pulsed dose-rate brachytherapy," *Med. Phys.* **22**, 821–829 (1995).

<sup>19</sup>P. Karaiskos, A. Angelopoulos, L. Sakelliou, P. Sandilos, C. Antypas, L. Vlachos, and E. Koutsouveli, "Monte Carlo and TLD dosimetry of an  $^{192}\text{Ir}$  high dose-rate brachytherapy source," *Med. Phys.* **25**, 1975–1984 (1998).

- <sup>20</sup>F. Ballester, V. Puchades, J. L. Lluch, M. A. Serrano-Andrés, Y. Limami, J. Calatayud-Pérez, and E. Casal, "Technical note: Monte-Carlo dosimetry of the HDR 12i and Plus  $^{192}\text{Ir}$  sources," *Med. Phys.* **28**, 2586–2591 (2001).
- <sup>21</sup>F. Ballester, V. Puchades, J. L. Lluch, M. A. Serrano-Andrés, Y. Limami, J. Calatayud-Pérez, and E. Casal, "Erratum: Technical note: Monte Carlo dosimetry of the HDR 12i and Plus  $^{192}\text{Ir}$  sources [Med. Phys. 28, 2586–2591 (2001)]," *Med. Phys.* **31**, 2372 (2004).
- <sup>22</sup>J. Pérez-Calatayud, F. Ballester, M. A. Serrano-Andrés, V. Puchades, J. L. Lluch, and Y. Limami, "Dosimetric characteristics of the Plus and 12i Gammamed PDR  $^{192}\text{Ir}$  source," *Med. Phys.* **28**, 2576–2585 (2001).
- <sup>23</sup>K. R. Russell, Å. K. Carlsson Tedgren, and A. Ahnesjö, "Brachytherapy source characterization for improved dose calculations using primary and scatter dose separation," *Med. Phys.* **32**, 2739–2752 (2005).
- <sup>24</sup>M. Ghiassi-Nejad, M. Jafarizadeh, M. R. Ahmadian-Pour, and A. R. Ghahramani, "Dosimetric characteristics of  $^{192}\text{Ir}$  sources used in interstitial brachytherapy," *Appl. Radiat. Isot.* **55**, 189–195 (2001).
- <sup>25</sup>I. Kawrakow and D. W. O. Rogers, "The EGSnrc code system: Monte Carlo simulation of electron and photon transport," National Research Council Canada Report No. PIRS-701, 2006.
- <sup>26</sup>J. Borg and D. W. O. Rogers, "Monte Carlo simulations of photon spectra in air from  $^{192}\text{Ir}$  sources," National Research Council Canada Report No. PIRS-629r, 1999.
- <sup>27</sup>D. W. O. Rogers, I. Kawrakow, J. P. Seuntjens, B. R. B. Walters, and E. Mainegra-Hing, National Research Council Canada Report No. PIRS-702 (revB), 2005.
- <sup>28</sup>M. J. Berger, J. H. Hubbell, S. M. Seltzer, J. Chang, J. S. Coursey, R. Sukumar, and D. S. Zucker, *XCOM: Photon Cross Section Database*, Version 1.3, National Institute of Standards and Technology, Gaithersburg, MD, 2005 [available online at <http://physics.nist.gov/xcom> (December 18, 2008)].
- <sup>29</sup>J. P. Seuntjens, I. Kawrakow, J. Borg, F. Hobeila, and D. W. O. Rogers, "Calculated and measured air-kerma response of ionization chambers in low and medium energy photon beams," in *International Workshop on Recent Developments in Accurate Radiation Dosimetry*, Montreal, Canada (Medical Physics, Madison, WI, 2002), pp. 69–84.
- <sup>30</sup>J. H. Hubbell and S. M. Seltzer, "Tables of x-ray mass attenuation coefficients and mass energy-absorption coefficients (version 1.4)." [Online] Available: <http://physics.nist.gov/xaamdi> [2009, April 21]. National Institute of Standards and Technology, Gaithersburg, MD (2004).
- <sup>31</sup>L. Antonovic, H. Gustafsson, G. Alm Carlsson, and Å. Carlsson Tedgren, "Evaluation of a lithium formate EPR dosimetry system for dose measurements around  $^{192}\text{Ir}$  brachytherapy sources," *Med. Phys.* **36**, 2236–2247 (2009).
- <sup>32</sup>G. M. Daskalov, E. Löffler, and J. F. Williamson, "Monte Carlo-aided dosimetry of a new high dose-rate brachytherapy source," *Med. Phys.* **25**, 2200–2208 (1998).
- <sup>33</sup>G. Daskalov, "Erratum: Monte Carlo-aided dosimetry of a new high dose-rate brachytherapy source [Med. Phys. 25, 2200–2208 (1998)]," *Med. Phys.* **27**, 1999 (2000).
- <sup>34</sup>P. Karaiskos, A. Angelopoulos, E. Pantelis, P. Papagiannis, L. Sakelliou, E. Kouwenhoven, and D. Baltas, "Monte Carlo dosimetry of a new  $^{192}\text{Ir}$  pulsed dose rate brachytherapy source," *Med. Phys.* **30**, 9–16 (2003).